A novel all-elastomer MEMS tactile sensor for high dynamic range shear and normal force sensing

A novel all-elastomer MEMS tactile sensor for high dynamic range shear and normal force sensing

Alexi Charalambides and Sarah Bergbreiter

Department of Mechanical Engineering and Institute for Systems Research, University of Maryland, 2181 Glenn L. Martin Hall, College Park, MD 20742, USA

E-mail: acharala@umd.edu and sarahb@umd.edu

CrossMark

Abstract

A novel all-elastomer MEMS tactile sensor with high dynamic force range is presented in this work. Conductive elastomeric capacitors formed from electrodes of varying heights enable robust sensing in both shear and normal directions without the need for multi-layered assembly. Sensor geometry has been tailored to maximize shear force sensitivity using multiphysics finite element simulations. A simple molding microfabrication process is presented to rapidly create the sensing skins with electrode gaps of 20 μm and sensor spacing of 3 mm. Shear force resolution was found to be as small as 50 mN and tested up to a range of 2 N (dynamic range of 40 : 1). Normal force resolution was found to be 190 mN with a tested range of 8 N (dynamic range of 42 : 1). Single load and multiload tests were conducted and the sensor exhibited intended behavior with low deviations between trials. Spatial tests were conducted on a 2 × 2 sensor array and a spatial resolution of 1.5 mm was found.

Keywords: polymer MEMS, 3-axis tactile sensor, high dynamic range

(Some figures may appear in colour only in the online journal)

1. Introduction

With recent advances in robotic manipulators, tactile sensing has had an increasing emphasis on compliant designs to accommodate curved surfaces such as robotic fingers. Remarkable progress has been made in the design and fabrication of flexible tactile sensors including multi-axis sensing, high sensor area density, and integration of elastomers with microfabrication [1, 2]. Some notable examples are presented in table 1 which contains performance metrics of each sensor.

One of the remaining challenges related to flexible tactile sensing is maintaining high dynamic range (DR) force sensing in both the shear and normal directions, where DR is defined in this work as force range divided by force resolution. As seen in table 1, achieving a large sensing range and small resolution in a single axis (shear or normal) is difficult, and achieving this in both sensing axes (shear and normal) has yet to be demonstrated. For in-hand manipulation tasks, Yousef defines an ideal sensor range up to 10 N with a resolution of

10 mN (DR = 1000 : 1) [1]. Typical ranges in table 1 are generally <1 N for shear force sensing and up to 5 N for normal force sensing. Dynamic ranges are even smaller for capacitive sensors (typical DR = 4 : 1).

Another challenge is to simplify fabrication in order to increase robustness, reduce costs, and improve manufacturing yield. The referenced tactile sensors in table 1 each have a multi-layered assembly which relies on an out-of-plane 'bump' structure to transfer shear forces to the sensing elements. This increases fabrication complexity, and can lead to failure at higher forces when the bump is made from a different, more rigid material [3].

The goal of this work is to create a tactile sensor capable of multi-axis sensing with high dynamic range while maintaining a compliant design with high spatial resolution similar to the human fingertip (1–2 mm [4]). To approach the above challenges, a rapid and simple microfabrication process is presented to reduce time and costs associated with previous tactile sensors while preserving high sensor area density. It

Table 1. Metrics of recent elastomeric shear and normal tactile sensors.

Publication	Type	Shear force			Normal force			Sensor Spacing (mm)	Bump Layer
		Range (mN)	Resolution (mN)	DR	Range (mN)	Resolution (mN)	DR		
Hwang [6]	Resistive	1470[a]	100[a]	15 : 1	4000	250[a]	16 : 1	2[a]	Yes
Lee [7]	Capacitive	20	3[a]	6.5 : 1	20	3[a]	6.5 : 1	2	Yes
Cheng [8]	Capacitive	108	26	4 : 1	108	26	4 : 1	8	Yes
Hu [9]	Resistive	500	25[a]	20 : 1	5000	150[a]	33 : 1	4.5[a]	Yes
Pyo [3]	Resistive	500	100[a]	5 : 1	2000	310[a]	6.5 : 1	8[a]	Yes
Ma [10]	Resistive	500[a]	50[a]	10 : 1	5000[a]	250[a]	20 : 1	4.5[a]	Yes
This work	Capacitive	2000	50	40 : 1	8000	190	42 : 1	3	No

[a] Value estimated based on figure or plot within publication.

improves the state-of-the-art by using electrode geometries of varying heights for capacitive sensing to improve force resolution and range, while maintaining 3-axis (shear and normal) force sensing without the need of an out-of-plane bump structure. It was designed using a multi-physics finite element model and tailored for shear sensing to achieve high dynamic range force sensing.

This paper builds on previous work [5], and presents a more detailed investigation of sensor material properties, governing geometric parameters, and the operation principle of shear sensing. Additional characterization of the sensor is also presented including 3-axis performance, combined loading behavior, spatial resolution tests, and incipient slip tests.

2. Sensor design

2.1. Architecture

Elastomeric materials were selected for the sensor due to their low elastic modulus and ability to withstand high strains. An inexpensive filler particle such as carbon can be added to create a conductive elastomer for the sensor electrodes. This alleviates the need for the deposition of a stiff metallic layer seen in previous sensors [6–8]. However, conductive elastomers suffer from resistance hysteresis when subject to strain [11, 12], and wiring to sensors is often subject to the same applied pressures and strains as the sensors; therefore capacitive sensing was selected as the preferred sensing method.

Capacitive tactile sensors have typically utilized parallel-plate style electrodes oriented orthogonal to the direction of applied force to transduce normal force or pressure; as a normal displacement is applied to the sensor, the distance between the two plates decreases and therefore increases capacitance [7, 8, 13–15]. Naturally, this technique requires multiple layers which can increase fabrication complexity. Capacitors with micron-scale air gaps between the electrodes are also limited in force range due to the collapse of the channel at low (sub 100 mN) forces [7, 8]. Sensor architecture is further complicated by the need for an out-of-plane bump structure to induce asymmetric deformation when the sensor is subject to shear forces.

In order to circumvent these complications, the proposed tactile sensor utilizes conductive elastomeric features of varying heights, *pillars* and *electrodes*, which enable predictable shear and normal deformation modes detectable using
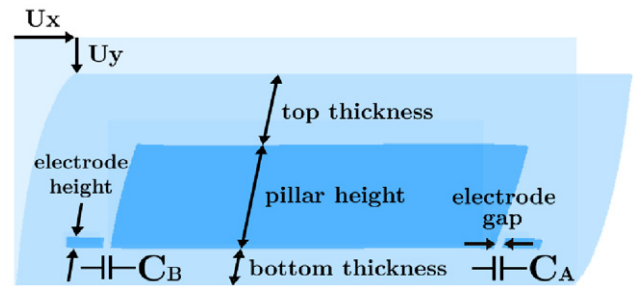
Figure 1. Proposed sensor architecture. Displacements U_x and U_y induce predictable changes in capacitance of C_A and C_B in order to detect normal and shear deformation modes.

capacitive sensing. Under shear loading, the pillar deforms towards one electrode and away from the other, figure 1, while under normal loading, the sensor flattens through Poisson's effect and the electrode gaps uniformly increase. Thus, the *capacitance differential* between the two electrode pairs, C_B–C_A, indicates the type of deformation occurring. These pairs of electrodes are placed in both shear directions in order to achieve 3-axis force sensing (2 shear, 1 normal). The conductive features are encased in a dielectric material with additional material on the top and bottom of the sensor for ease of fabrication and to protect the sensing elements. By avoiding air-gap capacitors the sensing range is only limited by the sensor material yield stress rather than the collapse of the air-gap. This feature substantially increases dynamic range over previous capacitive sensor designs (table 1).

2.2. Material properties

Uniaxial tension tests up to 50% strain were conducted for 10 wt.% carbon-polydimethylsiloxane (C/PDMS) composite and plain PDMS, figure 2, and were fit with first-order Ogden hyperelastic constitutive models [16] (materials and preperation can be found in section 3). The Ogden model was found to fit the experimental data more accurately than the Neo-Hookean or Mooney–Rivlin hyperelastic material models. The relationship between stress and strain (stretch ratio) is given by equations (1) and (2),

$$\sigma_{\text{Ogden}} = \mu(\lambda^{\alpha-1} - \lambda^{-0.5\alpha-1}) \tag{1}$$

$$\lambda = \varepsilon + 1 \tag{2}$$
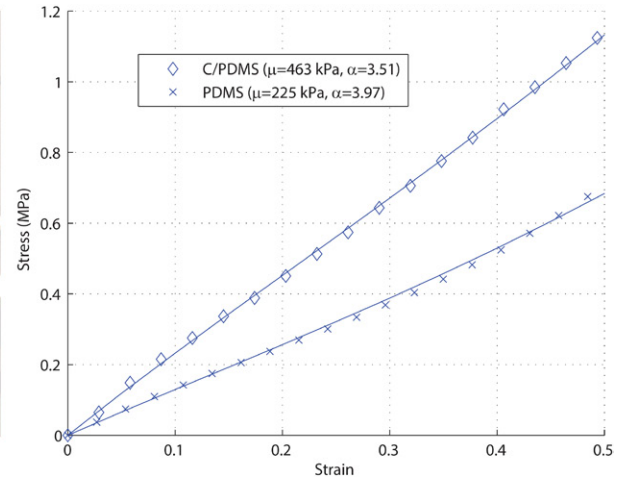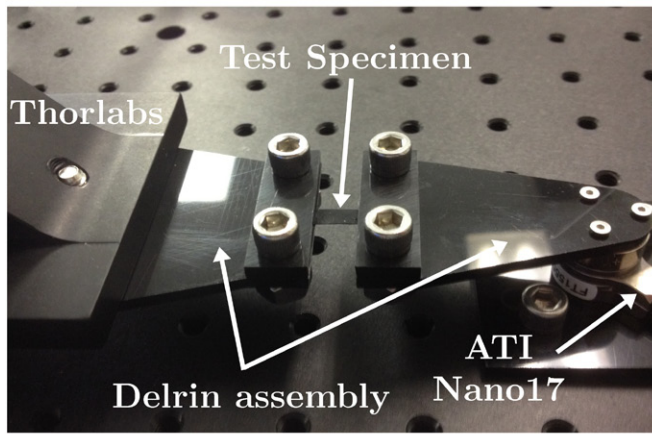
Figure 2. (Left) Uniaxial test setup for characterization of polymer composites. (Right) Stress–strain data for C/PDMS and PDMS with fitted 1st-order Ogden curves.

where σ_{Ogden} is Ogden stress, μ and α are first-order Ogden material properties, λ is stretch ratio, and ε is strain. The C/PDMS was found to have a slightly stiffer response than the PDMS which is consistent with the presence of a filler particle [17, 18]. A fairly linear response was observed in each material for these relatively low strains. For C/PDMS, a μ and α of 463 kPa and 3.51 were found, respectively, while for PDMS values of 225 kPa and 3.97 were found. These material properties were used in the subsequent finite element simulations.

2.3. Multiphysics finite element modeling

To guide design, 2D nonlinear large deformation finite element simulations were conducted using ANSYS to study the effect of sensor geometry on capacitance. An uncoupled multiphysics simulation based on [19] was developed such that: first, the geometry was mechanically deformed (element type PLANE182), and secondly, capacitance was solved using the CMATRIX command in the deformed configuration (element type PLANE121). A dielectric permittivity of 2.5 was assumed for PDMS. A fixed boundary condition was applied to the bottom edge, while X and Y displacements were applied to the top edge simulating shear and normal displacements respectively, figure 1.

Three parametric studies were conducted. First, the sensor was sheared and the capacitance differential was studied as a function of pillar and electrode height, figure 3. A large capacitance differential is preferable for shear force sensing. Second, the sensor's initial capacitance (i.e.: undeformed capacitance) was studied as a function of pillar and electrode height, figure 4. A high initial capacitance is preferable for normal force sensing [20]. From these two simulations, specific pillar and electrode heights were selected. Thirdly, the sensor was sheared using the selected pillar and electrode heights and the capacitance differential was studied as a function of the dielectric top and bottom thicknesses, figure 5.

In each figure, the Z-axis is in pF m^{-1} due to the 2D simulation, and the actual capacitance can be found by multiplying the out-of-plane electrode width, which in the fabricated design was 1 mm. Sensor thickness was arbitrarily selected
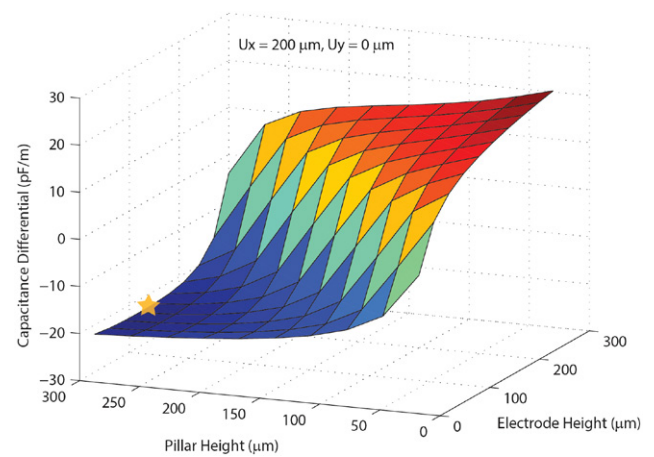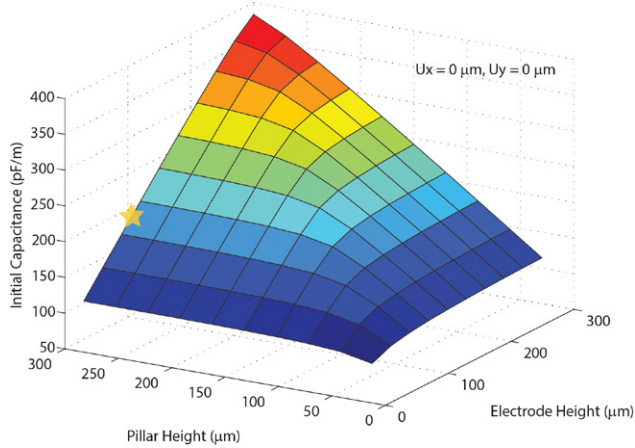

Figure 3. Finite element parametric study of the effects of pillar and electrode height on the capacitance differential when subject to shear displacement. The gold star is the geometry selected.

for the simulations in figures 3 and 4; bottom thickness was 100 μm, and the sum of the top thickness and pillar height was held constant at 500 μm. Preliminary simulations revealed that smaller electrode gaps resulted in larger changes in capacitance, so an electrode gap of 20 μm was selected; it was also the smallest gap that could be consistently fabricated. A simulated shear displacement of 200 μm was selected as a benchmark of performance.

In figure 3, two extreme regions were found: a tall pillar and short electrode (blue region), and vice versa (red region). In addition, when the pillar height equals the electrode height, a capacitance differential of zero is found (green region). Therefore, the difference in height between the pillar and electrode is what enables shear sensing. By contrast, for normal sensing it was found that a large pillar height and electrode height lead to the highest initial capacitance, figure 4. Due to the competing phenomena, a geometry that maintains both high capacitance differential and sufficient initial capacitance was selected, as represented by the gold stars in figures 3 and 4; electrode height was 100 μm, and pillar height was 300 μm.

In figure 5, the simulation that exhibited the highest strain of 24% was for a bottom and top thickness equal to 100 μm;

Figure 4. Finite element parametric study of the effects of pillar and electrode height on initial (undeformed) capacitance. The gold star is the geometry selected.
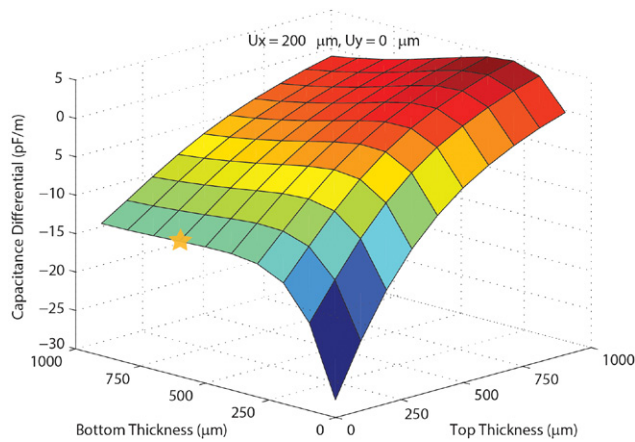
Figure 5. Finite element parametric study of the effects of top and bottom thickness on capacitance differential when subject to shear displacement. The gold star is the geometry selected.

this was about half of the maximum strain tested in section 2.2. This point corresponded to the highest capacitance differential. However, a large bottom thickness improves the ability to peel the device from the silicon mold without risking a tear during fabrication, as described in section 3, thus a bottom and top thickness of 600 μm and 100 μm, respectively, were selected as represented by the gold star in figure 5.

2.4. Shear sensing mechanism

To better understand how capacitance changes during shear deformation, the proposed sensor was divided into three areas in which the electrostatic energy changes as a shear displacement is applied, figure 6. As a shear displacement is applied toward the right, the pillar deforms over the electrode which increases the electrostatic energy in the *Overlap* area while also increasing the energy in between the electrodes, the *Gap* area. The *Underlying* area was found to slightly decrease in energy and makes little contribution to the overall change in capacitance. A linear and nonlinear change in capacitance was observed in the *Overlap* and *Gap* areas, respectively, indicating that at lower shear displacements a relatively linear

change in capacitance is expected. The areas on the left side of the pillar in figure 6 were found to behave similarly, but decrease in capacitance rather than increase.

3. Microfabrication

Sensors were made from a reusable silicon mold, which was fabricated using a two mask microfabrication process, figure 7. Silicon dioxide was deposited on a silicon wafer, patterned, and etched with the first mask containing the pillar geometry. A second pattern and partial oxide etching was done using the second mask, which contained the electrode and electrical lead geometries. Next, an oxygen plasma was used to clean the surface of photoresist, followed by a deep reactive ion etch (DRIE) to create the mold, which was finally coated with a DuPont amorphous fluoroplastic solution (Grade 400S2) as an antistick agent. This completed the reusable silicon mold.

10 wt.% C/PDMS was prepared by mixing 1 g of carbon black powder (39724, Alfa Aesar), 8.18 g of PDMS base and 0.818 g of PDMS curing agent (Sylgard 184, Dow Corning), and 22.5 g of hexane for 30 min. It was poured on the mold, vacuumed for 2 min at 1 Torr, planarized by hand using an industrial screen printing squeegee (Ryonet), and cured on a hot plate for 15 min at 120 °C. After curing, a layer of PDMS was poured on the mold, vacuumed for 15 min at 1 Torr, and cured on a hot plate for 15 min at 120 °C. The vacuum step served to both degas and gravity level the PDMS while controlling the layer thickness. Then, the elastomeric sensor was peeled from the wafer as one whole piece. Lastly, the sensing area was encapsulated in another layer of PDMS using the aforementioned process, and resulted in a total sensor thickness of 1.06 mm. The final all-elastomer sensor can be seen in figure 7 (Bottom right).

## 4. Experimental results

4.1. Test setup

Testing was conducted by applying a displacement to the sensor and reading the capacitances of each electrode as well as the reaction forces. Micron-scale displacements were applied using a Thorlabs PT3-Z8 3-axis stage equipped with a laser cut delrin probe which had a square probe tip area of 3×3 mm. Capacitance was measured using an AD7745/46 evaluation board with an observed resolution of 0.1 fF at a sampling rate of 16 Hz (unless otherwise noted). Forces were acquired using an ATI Nano17 6-axis force/torque sensor, and the assembled test setup can be seen in figure 8 (Left).

4.2. Results

4.2.1. Signal behavior. The data from the ATI sensor and fabricated tactile sensor via the AD evaluation board exhibited step-like behavior in the time domain when subject to incremental displacements, figure 8 (Right). At higher force readings, a slight decay is apparent in the ATI signal which may be due to polymer relaxation in the sensor, so the median value over the step was used.
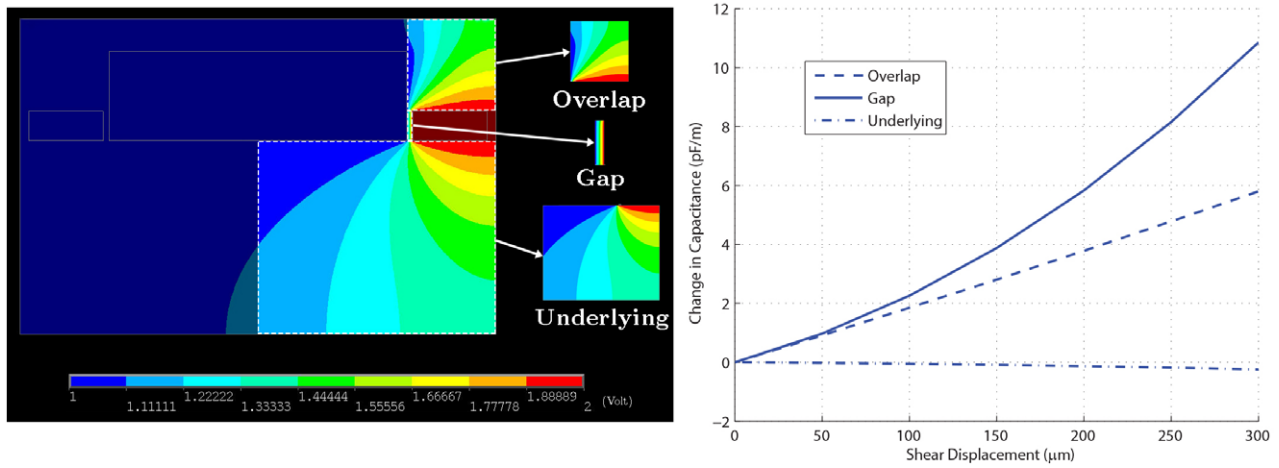
Figure 6. (Left) Sensor areas in which electrostatic energy changes as the sensor deforms. (Right) Finite element results of the change in capacitance of each area when subject to shear displacement.
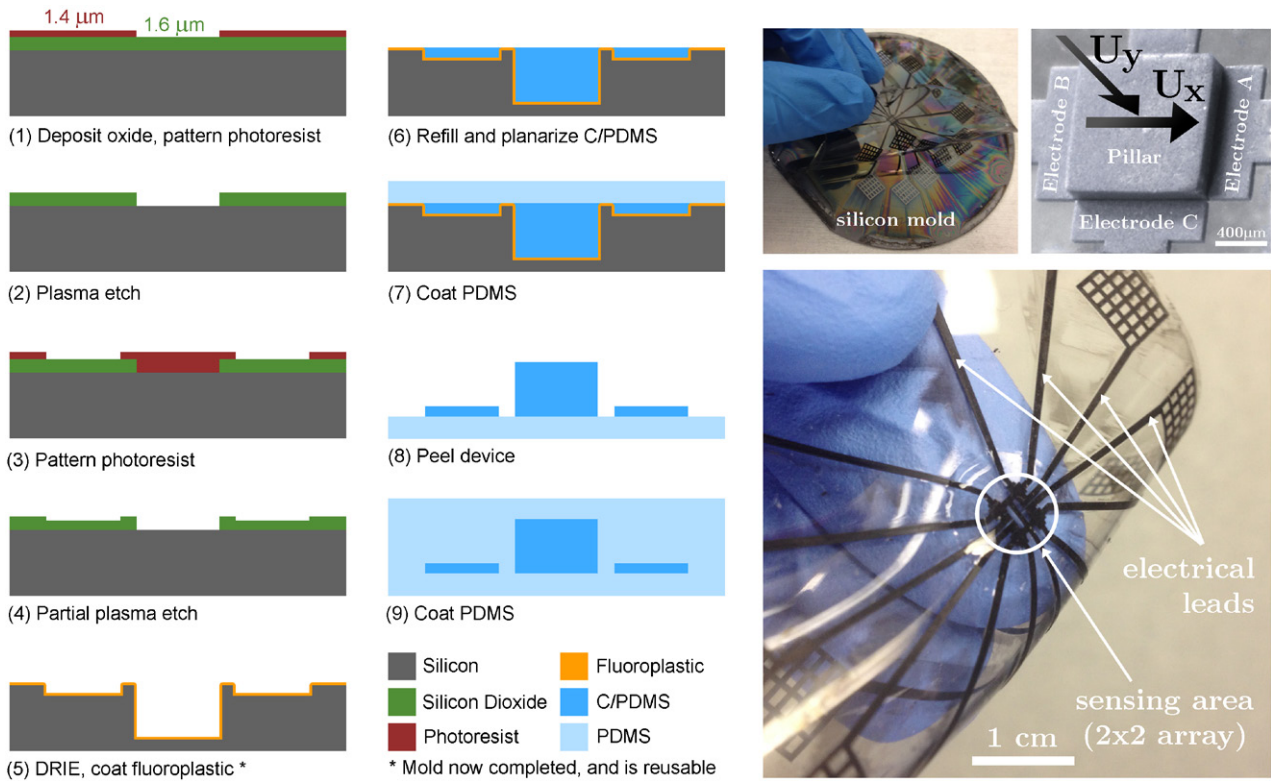

Figure 7. (Left) Microfabrication flow chart. (Top off-center) Peeling of the fabricated sensor from the silicon mold. (Top right) Macro photo of a single pillar and surrounding electrodes. This image has been edited for clarity. (Bottom right) Completed sensor in hand.

4.2.2. Shear force resolution. Shear force resolution was determined by conducting incremental shear displacement tests. Increments of 10 μm shear displacements were applied up to 100 μm in the positive U_x direction as seen in figure 7 (Top right).

A pre-applied normal force was necessary to sense shear in order to avoid slip between the probe tip and sensor; without normal force, the probe and sensor are not in contact. In this test and subsequent tests where a normal force preload is used, a normal displacement on the order of 10's of μm was applied to the probe which resulted in normal forces between 1.5 and 2 N. This is a realistic force range seen in robotic grasping [21].

The sensor exhibited a linear capacitive response up to 700 mN shear force, figure 9. As intended, Electrode A increased in capacitance, Electrode B decreased, while Electrode C remained relatively constant. Figure 9 plots the experimental results along with ANSYS results for the same normal and shear forces. The finite element model predicts a nonlinear response in this range and the deviation between the model and experiment at higher shear force values is possibly due to alignment errors during fabrication or unmodeled changes in material properties. A shear force resolution of 50 mN was observed for Electrode A based on the minimum shear displacement tested (10 μm).
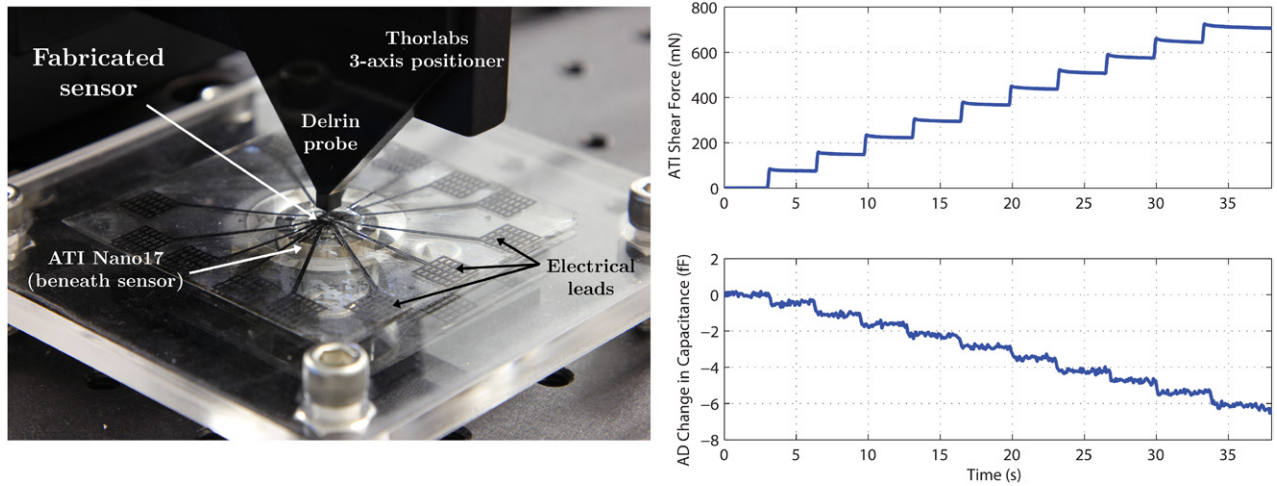
Figure 8. (Left) Test setup of the Thorlabs and ATI equipment. The AD7745/46 capacitive board, not shown, has pen-style probes which may be pressed against the fabricated sensor's electrical leads to acquire data. (Right) Sample raw data from the ATI sensor and the AD7745/46 evaluation board. Steps are increments of 10 μm of shear displacement.
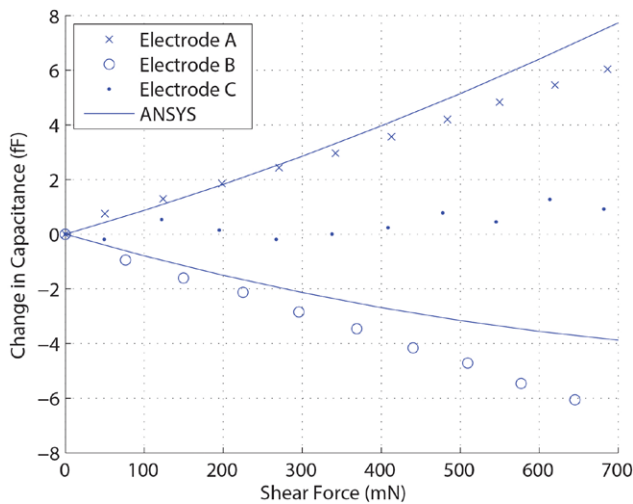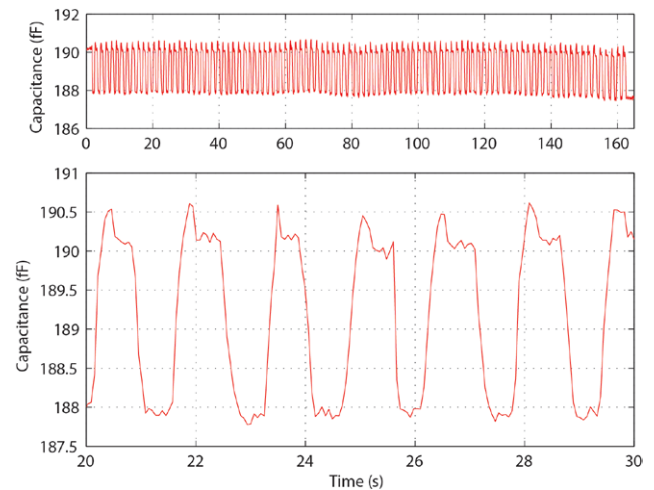

Figure 9. High resolution shear testing compared to the finite element model. Each data point was gathered after a shear displacement of 10 μm was applied.

Figure 10. Cyclic testing of Electrode B over 100 cycles of 100 μm shear displacement. A detailed view of the signal reveals overshoot from the Thorlabs controller.

4.2.3. Cyclic loading. Cyclic testing was conducted for a 100 μm shear displacement while a high normal force of 10 N was applied in order to assess any sensor hysteresis, figure 10, and data from Electrode B was collected. At 100 cycles over 160 s, no hysteresis was observed, and the signal remained clear enough to discern overshoot from the Thorlabs stage controller during the return step of each cycle.

4.2.4. 3-axis performance. A single sensor from the tactile skin was selected, and was displaced in 5 Cartesian directions (4 shear, 1 normal) with 5 trials in each direction. Data from each of the 3 electrodes was collected resulting in 75 total capacitance-force relationships, figure 11.

In the shear tests, figures 11(a)–(d), increments of 50 μm displacements were applied up to 250 μm after a normal force preload was applied. As intended, capacitances of electrodes parallel to the direction of applied shear changed little compared to adjacent electrodes. This indicates an ability to differentiate the direction of applied shear force. Measured

capacitance and force readings were consistent between trials, suggesting a highly repeatable behavior.

In the normal tests, figure 11(e), increments of 30 μm displacements were applied up to 150 μm. A decrease in capacitance was observed in each electrode consistent with previously observed behavior [5, 20]. A normal force resolution of 190 mN was observed for Electrode C based on the minimum normal displacement tested (30 μm). The change in capacitance of the normal tests was less than that of the shear tests per force (i.e.: lower sensitivity). This is an expected outcome since the sensor was designed to maximize capacitance differential under shear, and maximizing initial capacitance was secondary (section 2.3).

4.2.5. Mixed loading. Capacitance contours of each electrode were collected over an array of shear and normal forces, figure 12. This test also included the maximum ranges applied (2 N in shear and 8 N normal), although sensors were not tested to failure. One trial per load case was
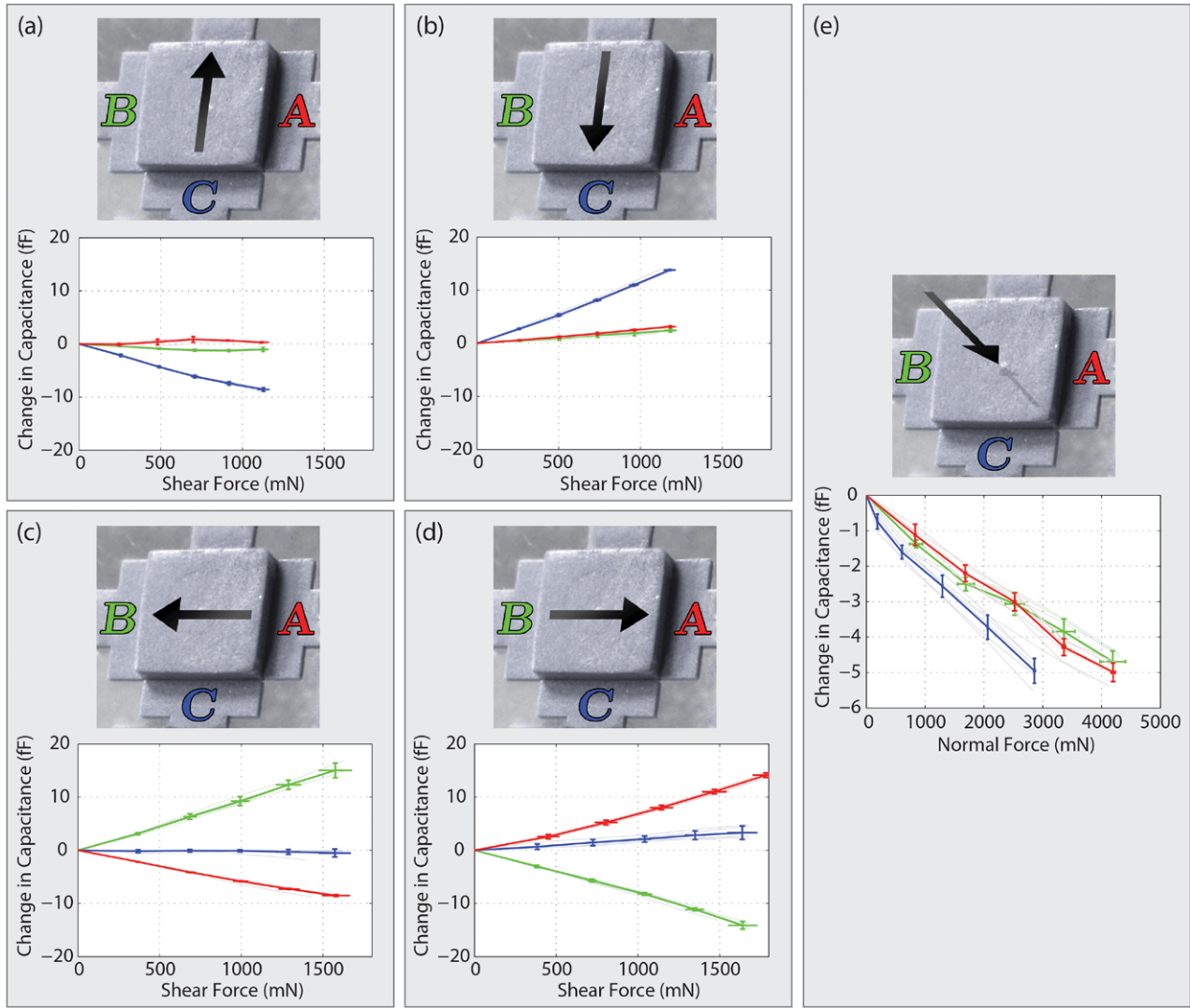
Figure 11. 3-axis tests in each direction and the response of each electrode, A (red), B (green), and C (blue). (a)–(d) For shear testing, increments of 50 μm displacement were applied up to 250 μm. (e) For normal testing, increments of 30 μm displacement were applied up to 150 μm. Force (horizontal) and capacitance (vertical) deviation bars are for one pillar tested over 5 trials. The photos adjacent to each plot have been edited for clarity.
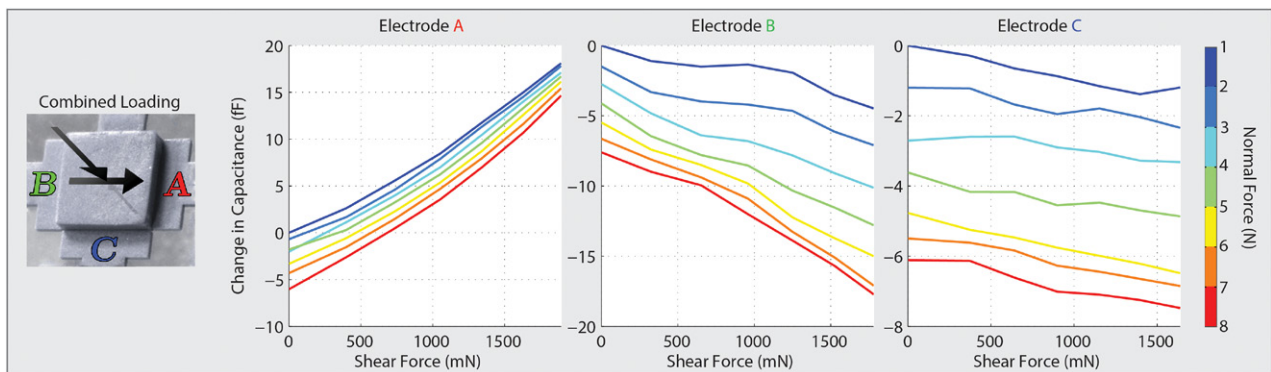

Figure 12. Mixed loading performance of each electrode when subject to simultaneous shear and normal forces. One trial per load case was conducted. The adjacent photo has been edited for clarity.

conducted. A decrease in capacitance was observed in all electrodes as a normal force was applied, as intended. Each electrode behaved as expected when subject to shear regardless of applied normal force. Electrode C, which was oriented

parallel to the direction of applied shear, exhibited a slight decrease in capacitance as shear force was applied. Sensor sensitivity to shear was found to be relatively independent of normal force. Using this information, the change in
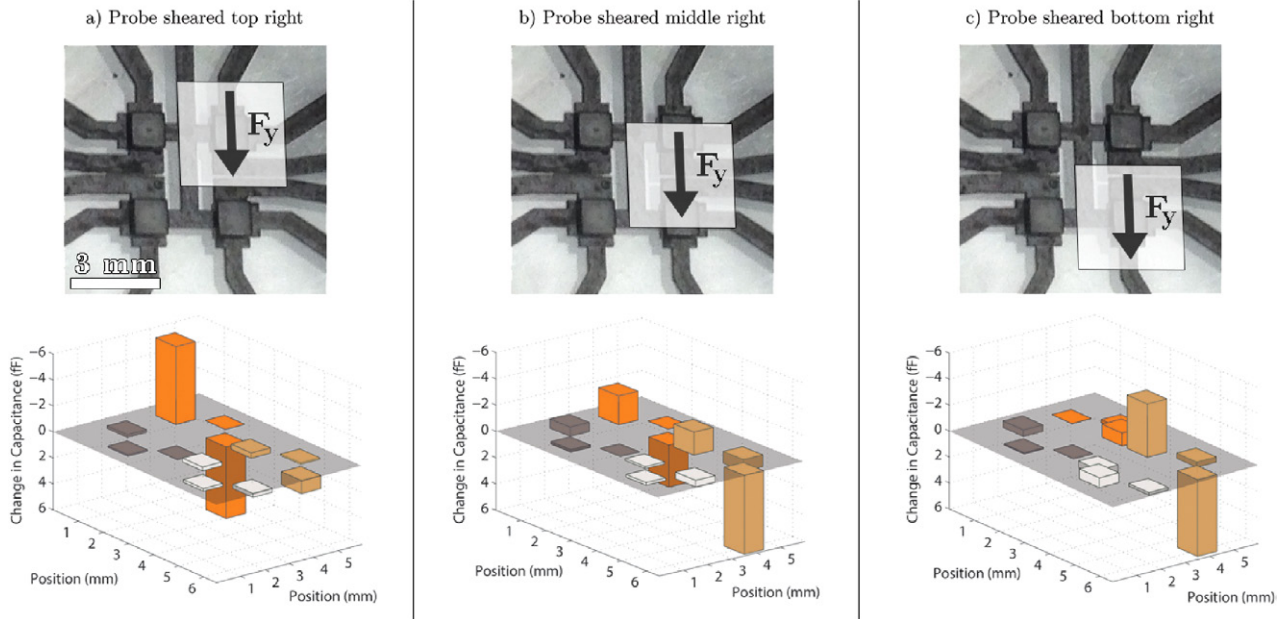
Figure 13. Spatial resolution tests in which a 700 mN shear force was applied at three different locations each 1.5 mm apart. (a) Probe centered over the top right pillar. (b) Probe placed between the two right pillars. (c) Probe placed over the bottom right pillar.

capacitance of each electrode can be used to infer the type of deformation occurring. For example, a nonzero capacitance differential across two opposite electrodes indicates shear occurring, while a net decrease of each electrode indicates the presence of an applied normal force. A detailed predictive model for applied forces given these capacitive changes is subject to further work.

4.2.6. Spatial resolution. A shear force of 700 mN was applied at three locations, each 1.5 mm apart, and the change in capacitance of each electrode was collected, figure 13. The tactile skin contained 4 pillars with 3 electrodes each yielding 12 total measurements. A preload normal force was applied prior to each test.

The electrodes that experienced changes in capacitance were observed to correspond with the location of the probe, while near-zero changes in capacitance were observed elsewhere. This suggests low spatial crosstalk and a minimum spatial resolution of 1.5 mm using the tested probe (i.e.: the minimum change in position of the probe detectable was 1.5 mm).

4.2.7. Incipient slip. In order to investigate the sensor's ability to detect incipient slip which is important to robotic grasping [22], a preload normal force was applied followed by a high shear displacement of greater than 1 mm to induce slip between the sensor and probe, figure 14. Capacitance was collected from Electrode B at a sampling frequency of 90 Hz, which was the maximum frequency of the AD evaluation board. Upon initial loading, a decrease in capacitance can be seen as expected, figure 14 Region (II). Then, a sudden increase and oscillation in the signal was observed upon initiation of slip, figure 14 Region (III). The signal was filtered using an 11-point moving average to more clearly display the data trends.
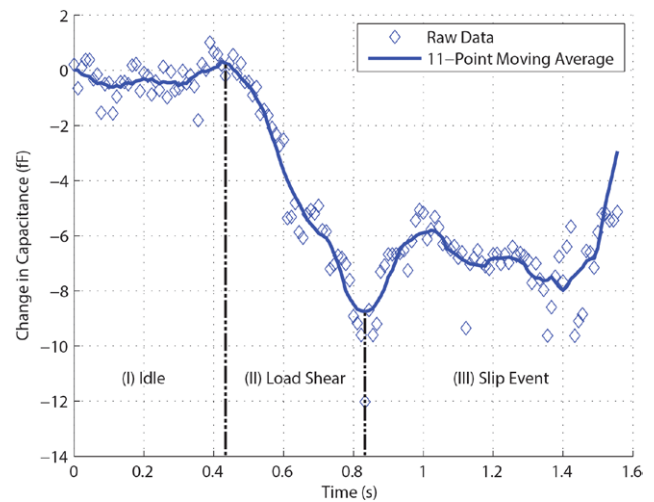
Figure 14. Incipient slip test. As the sensor is sheared, Region (II), slip is observed near $t = 0.8$ s. The 11-point moving average increases suddenly and jitters over a range of several fF in Region (III). A sampling rate of 90 Hz was used.

5. Limitations and future work

One limitation of this sensor was the lack of a readily available high conductivity composite polymer. Due to this reason, electrical routing from the electrodes and pillars had to be significantly wider than anticipated, which left no available space for a fourth electrode to oppose Electrode C. A high conductivity composite polymer, such as silver-polydimethylsiloxane (Ag/PDMS) [23], may potentially solve this issue; it was also utilized in previous work [20], but has since been difficult to incorporate in fabrication due to its tendency to separate after mixing.

Another challenge was the use of in-plane wiring which significantly reduced the ability to create an array larger than

2×2. An additional backing layer, such as polyimide, with protruding electrical leads to penetrate the C/PDMS may be necessary in the future to expand the array.

6. Conclusion

A novel all-elastomer MEMS tactile skin has been presented, which utilizes electrode geometries of varying heights to sense both shear and normal forces without the need of an out-of-plane bump. The tactile skin was fabricated using a simple and rapid molding process while maintaining high sensor area density, with sensors spaced every 3 mm. A high dynamic shear and normal force range was achieved of $40 : 1$ and $42 : 1$, respectively, which is the highest reported of elastomeric 3-axis sensors thus far. This was achieved through the guidance of a finite element model to tune the tactile skin for shear sensing. Future work could utilize a higher conductivity polymer to decrease feature size and increase sensor area density further.

Acknowledgment

References

[1] Yousef H, Boukallel M and Althoefer K 2011 Tactile sensing for dexterous in-hand manipulation in robotics: a review *Sensors Actuators* A **167** 171–87

[2] Dahiya R S, Metta G, Valle M and Sandini G 2010 Tactile sensing from humans to humanoids *IEEE Trans. Robot.* **26** 1–20

[3] Pyo S, Lee J I, Kim M-O, Chung T, Oh Y, Lim S-C, Park J and Kim J 2014 Development of a flexible three-axis tactile sensor based on screen-printed carbon nanotube-polymer composite *J. Micromech. Microeng.* **24** 075012

[4] Dargahi J and Najarian S 2004 Human tactile perception as a standard for artificial tactile sensing: a review *Int. J. Med. Robot. Comput. Assist. Surg.* **1** 23–35

[5] Charalambides A, Cheng J, Li T and Bergbreiter S 2015 3-axis all elastomer mems tactile sensor *28th IEEE Int. Conf. on Micro Electro Mechanical Systems* pp 726–9

[6] Hwang E-S, Seo J-H and Kim Y-J 2007 A polymer-based flexible tactile sensor for both normal and shear load detections and its application for robotics *J. Microelectromech. Syst.* **16** 556–63

[7] Lee H-K, Chung J, Chang S-I and Yoon E 2011 Real-time measurement of the three-axis contact force distribution using a flexible capacitive polymer tactile sensor *J. Micromech. Microeng.* **21** 035010

[8] Cheng M-Y, Lin C-L, Lai Y-T and Yang Y-J 2010 A polymer-based capacitive sensing array for normal and shear force measurement *Sensors* **10** 10211–25

[9] Hu C-F, Su W-S and Fang W 2011 Development of patterned carbon nanotubes on a 3d polymer substrate for the flexible tactile sensor application *J. Micromech. Microeng.* **21** 115012

[10] Ma C-W, Hsu L-S, Kuo J-C and Yang Y-J 2014 A flexible tactile and shear sensing array fabricated using a novel buckypaper patterning technique *Sensors Actuators* A **231** 21–7

[11] Ventrelli L, Beccai L, Mattoli V, Menciassi A and Dario P 2009 Development of a stretchable skin-like tactile sensor based on polymeric composites *IEEE Int. Conf. on Robotics and Biomimetics* pp 123–8

[12] Gerratt A P and Bergbreiter S 2012 Microfabrication of compliant all-polymer mems thermal actuators *Sensors Actuators* A **177** 16–22

[13] Chase T A and Luo R C 1995 A thin-film flexible capacitive tactile normal/shear force array sensor *Proc. of the 1995 IEEE IECON 21st Int. Conf. on Industrial Electronics, Control, and Instrumentation* vol 2 pp 1196–201

[14] Rocha J G, Santos C, Cabral J M and Lanceros-Mendez S 2006 3 axis capacitive tactile sensor and readout electronics *IEEE Int. Symp. on Industrial Electronics* vol 4 pp 2767–72

[15] Lipomi D J, Vosgueritchian M, Tee B C K, Hellstrom S L, Lee J A, Fox C H and Bao Z 2011 Skin-like pressure and strain sensors based on transparent elastic films of carbon nanotubes *Nat. Nanotechnol.* **6** 788–92

[16] Ogden R W 1997 *Non-Linear Elastic Deformations* (Mineola, NY: Courier Corporation)

[17] Goyal A, Kumar A, Patra P K, Mahendra S, Tabatabaei S, Alvarez P J J, John G and Ajayan P M 2009 In situ synthesis of metal nanoparticle embedded free standing multifunctional pdms films *Macromol. Rapid Commun.* **30** 1116–22

[18] Frogley M D, Ravich D and Wagner H D 2003 Mechanical properties of carbon nanoparticle-reinforced elastomers *Compos. Sci. Technol.* **63** 1647–54

[19] Yang Z, Li G, Hao Y and Wu G 2004 Dynamic capacitance extraction of a triaxial capacitive accelerometer *Int. ANSYS Conf.*

[20] Charalambides A and Bergbreiter S 2013 All-elastomer in-plane mems capacitive tactile sensor for normal force detection *IEEE Sensors* pp 1–4

[21] Howe R D 1993 Tactile sensing and control of robotic manipulation *Adv. Robot.* **8** 245–61

[22] Bicchi A and Kumar V 2000 Robotic grasping and contact: a review *IEEE Int. Conf. on Robotics and Automation* pp 348–53

[23] Niu X Z, Peng S L, Liu L Y, Wen W J and Sheng P 2007 Characterizing and patterning of pdms-based conducting composites *Adv. Mater.* **19** 2682–6